# Multimodal optical non-destructive evaluation of impact damage in composite materials

D. Budiakivska*[a], N. Tao[b], A. Styk[a], M. Kujawińska[a], A. Anisimov[b]

[a]Warsaw University of Technology, Institute of Micromechanics and Photonics, 02-525 Warsaw, 8 Sw. A. Boboli St., Poland;
[b]Delft University of Technology, Aerospace Structures and Materials Department, Kluyverweg 1, 2629 HS, Delft, The Netherlands

## ABSTRACT

Structural integrity of composite materials is vital for aerospace applications, requiring advanced non-destructive inspection (NDI). This study combines shearography and digital image correlation (DIC) to assess carbon-fiber reinforced polymer (CFRP) samples after the impact. Impact testing via a drop tower induced different damage types, detected by both techniques. Four-point bending test enhanced defect visibility. The measurements were performed by shearography and 3D DIC using the same cameras from the 3D shearography system. Shearography identified defects earlier than DIC, while DIC offered bigger range of displacements and strain measurements highlighting the complementary role of both methods and multimodal NDI test's effectiveness in detecting impact damage and manufacturing defects.

**Keywords:** Composites, shearography, non-destructive inspection, digital image correlation

## 1. INTRODUCTION

Non-destructive inspection (NDI) is a crucial continuously developing field for testing of various structures and elements. Many different techniques are considered to be NDI, including digital image correlation (DIC), electronic speckle pattern interferometry (ESPI), structured light projection, shearography[1], ultrasonic testing, and many more[2]. Composite materials are present in many areas of our everyday life, including, but not limited to aerospace, automotive, architecture, sports, infrastructure. Such wide usage raised the necessity for searching and broadening the ways of the inspection. The challenges associated with the composites inspection include complex geometry, anisotropy, making it hard to achieve perfect results with just a single inspection technique[2]. Multimodality allows to combine advantages of different testing techniques, helping to confront problems in a different way at the same time. However, several gaps and challenges persist in the current implementation of multimodal optical systems. Although many studies have demonstrated promising proof-of-concept experiments, they often lack robust and standardized frameworks for integrating hybrid data acquisition and processing[3].

Furthermore, while the combination of multiple optical techniques holds promise, its application to the inspection of impact-induced damage remains limited. Much of the existing research has concentrated on quasi-static loading or long-term creep behaviour, with less emphasis on post-impact evaluation scenarios. Although dynamic, real-time monitoring during impact presents additional challenges[4], even post-impact inspections face practical issues such as the need for precise calibration, spatial alignment, and system synchronization – all of which can affect measurement accuracy and usability. Moreover, many current multimodal setups are not optimized for efficient inspection workflows, especially when high throughput or rapid assessments are required in practice.[2]

*darynabudiakivska@gmail.com

Multimodal Sensing and Artificial Intelligence for Sustainable Future, edited by Francesco Soldovieri, Pascal Picart, Vittorio Bianco, Claas Falldorf, Proc. of SPIE Vol. 13570, 1357026
2025 Published by SPIE · 0277-786X · doi: 10.1117/12.3066629

Several studies have attempted to integrate two or more optical NDI techniques to increase their individual strengths. In the study by Malesa et al. (2019)[3], a hybrid GI-DIC (grating interferometry) measurement procedure was developed to assess strain fields at different spatial resolutions. GI offers high sensitivity to micro-scale strain gradients, while DIC provides macro-scale full-field strain mapping. Their integration enabled a hierarchical evaluation, where GI focused on local damage indicators (e.g., high strain concentrations), and DIC complemented with global deformation behaviour. Pascual-Francisco et al. (2017)[5] explored the combined use of shearography and DIC to study creep behaviour in elastomers. While shearography revealed areas of internal defect evolution, DIC allowed quantification of the surface strain. The study demonstrated the complementarity of the methods in identifying both subsurface anomalies and surface deformation during long-term loading. Although the work focused on creep rather than impact, it validated the dual-modal synergy for enhanced material characterization.

Despite these advancements, multimodal optical NDI systems are still not widely applied to evaluate impact damage in composite structures. Impact loading often results in complex, hierarchical damage patterns including matrix cracks, fiber breakage, and delamination. These features may span different length scales and depths, requiring both surface-sensitive and subsurface-sensitive techniques. For the case of structural integrity analysis of composite materials, we propose to combine two full-field optical techniques which provide strain distribution in investigated samples, namely shearography[6] and digital image correlation[7] methods. Both of them have their advantages and disadvantages, but also complement each other in the sensitivity, allowed range of deformation and strains, signal to noise ratio and measurement requirements and therefore might provide better experimental results. Our aim is to enhance a hybrid DIC-shearography framework specifically tailored to detect and characterize impact-induced damage in composite materials. This approach seeks to bridge the gap between qualitative defect detection and quantitative mechanical assessment, ultimately contributing to more reliable and comprehensive structural health monitoring.

Standard loading types applied during shearography measurement are thermal excitation (typically with halogen lamps)[8], mechanical, vibrations or vacuum[9]. In this study, the goal was to compare the ability of DIC and shearography to detect mechanically induced strain introduced by four-point bending with is described by Y. Khan (2019)[10], M. Hun et al. (2012)[11], and others[12].

## 2. SAMPLE STRUCTURE AND PROPOSED METHODOLOGY

During the experiment carbon-fiber reinforced polymer (CFRP) HexPly as4 8552 (prepreg cured in autoclave) samples with orthotropic (OR) layup [45/0/0/-45/0/0/45/0/-45/0/0/90]s (24 layers) were measured (Figure 1(a)). Impact was performed with a drop tower as shown in Figure 1(b) with calibrated impact energy range varying from 18 to 48J. Before the experiment the DIC-Shearography measurements samples were coated with a base layer of white scattering paint and the second speckled layer of black acrylic paint – to ensure unique speckle pattern on the surface. Further, strain gauges were bonded to the surface at a side, not to disturb the optical measurements. In Figure 1(c) the samples are presented with energy of the impact growing from left to right as follows: OR1.5 – 27.33J, OR2.5 – 36.65J, OR2.8 – 45.89J, where ORx.y is an internal specimen naming. The main goal of the investigations was to track, how well shearography detects the damage for different impact energies and at what load would 3D DIC start detecting the same damage.

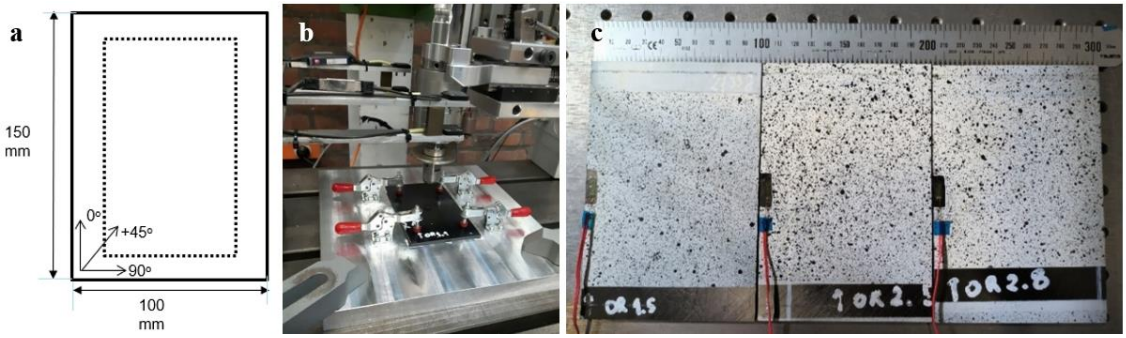


Figure 1: (a) Sample layout, (b) Drop tower facility at Delft University of Technology, (c) Samples prepared to be measured with attached strain gauges.

The loading process was performed stepwise, where for shearography the steps were approximately equal to 40 με in $\varepsilon_{yy}$ direction, while for 3D DIC the steps were 135 με in $\varepsilon_{yy}$ direction.

## 3. METHODS AND EXPERIMENTAL SETUPS

### 3.1 Shearography

Shearography is a full-field laser-based non-destructive inspection optical technique that provides full-field surface strain characterization. Its sensitivity to deformation gradients makes it particularly effective for identifying subsurface defects such as delaminations, disbonding, and inclusions in composite structures. Traditional shearography systems primarily measure the out-of-plane strain components, but recent advancements have enabled three-dimensional (3D) deformation measurements, significantly improving the technique's diagnostic capability – especially for complex geometries and curved surfaces[13].

In this study, an in-house built 3D shearography system from Delft University of Technology was employed (Figure 2(a)), offering enhanced functionality beyond standard commercial systems. The setup includes four synchronized Basler piA2400-12gm 2456x2058 pixels cameras: three arranged to perform 3D shearography, enabling the separation of the in-plane and out-of-plane strain components, and a fourth camera dedicated solely to capturing pure out-of-plane deformations. Each camera is equipped with a Michelson interferometer operating under temporal phase-shifting conditions, allowing for high-precision phase difference acquisition. The spatial resolution of the system during this experiment is equal to 108 µm. In this study, only cameras 1 and 3 (Figure 2(a)) were used to record the in-plane and out-of-plane strain components in the $x$ (horizontal) direction ($\varepsilon_{xx}$, $\frac{\partial w}{\partial x}$, in alternative form $\frac{\partial u_z}{\partial x}$). The system supports dual excitation modes: thermal loading, achieved via three halogen lamps (each rated at 1 kW), and mechanical loading, which is tailored to individual specimen designs (non-vacuum-based). Additionally, an infrared (IR) FLIR Systems AX5 camera is integrated into the setup to monitor the surface temperature evolution during thermal loading, ensuring controlled and consistent excitation. The system's flexibility allows for different fields of view: ranging from 100×100 mm² to 500×500 mm² in single-camera mode, and up to 200×200 mm² in 3D shearography mode, making it suitable for detailed inspections across a range of specimen sizes. Available laser sources include a 200 mW 532 nm and a more powerful 6 W option, depending on the measurement sensitivity and illumination area required[6]. A fixed frame was placed in the distance of 60 cm from the laser source to safely and rigidly apply four-point bending technique to the sample (Figure 2(b)).

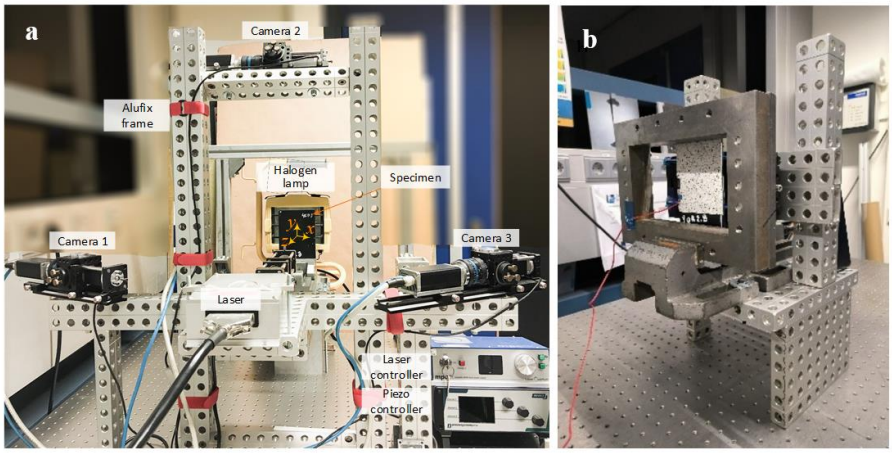


Figure 2: (a) Utilized Shearography and DIC measurement system, (b) Sample mounting setup with four point bending loading mechanism

Image recording and system control are performed in a custom National Instruments LabVIEW program. It allows for precise control over variables like shear distance, time delays, heating times, phase shifting algorithms, etc. After recording, interferograms are processed in the MATLAB application, where phase is calculated. As more than one camera is utilized, stereo image rectification is used to project images onto common image plane. As the output a set of images representing infinitesimal strain tensor variables (Equation 1) are calculated. The main importance for the research presented the $\frac{\partial u_x}{\partial x}$ as it can be assumed to be equal to $\varepsilon_{xx}$ for the cases when the deformations are small and $\frac{\partial u_z}{\partial x}$, in further study denoted as $\frac{\partial w}{\partial x}$.

$$\begin{bmatrix} \varepsilon_{xx} & \varepsilon_{xy} & \varepsilon_{xz} \\ \varepsilon_{yx} & \varepsilon_{yy} & \varepsilon_{yz} \\ \varepsilon_{zx} & \varepsilon_{zy} & \varepsilon_{zz} \end{bmatrix} = \begin{bmatrix} \frac{\partial u_x}{\partial x} & \frac{1}{2}\left(\frac{\partial u_x}{\partial y} + \frac{\partial u_y}{\partial x}\right) & \frac{1}{2}\left(\frac{\partial u_x}{\partial z} + \frac{\partial u_z}{\partial x}\right) \\ \frac{1}{2}\left(\frac{\partial u_y}{\partial x} + \frac{\partial u_x}{\partial y}\right) & \frac{\partial u_y}{\partial y} & \frac{1}{2}\left(\frac{\partial u_y}{\partial z} + \frac{\partial u_z}{\partial y}\right) \\ \frac{1}{2}\left(\frac{\partial u_z}{\partial x} + \frac{\partial u_x}{\partial z}\right) & \frac{1}{2}\left(\frac{\partial u_z}{\partial y} + \frac{\partial u_y}{\partial z}\right) & \frac{\partial u_z}{\partial z} \end{bmatrix} \quad (1)$$

### 3.2 3D DIC

3D Digital Image Correlation is a widely adopted non-contact, non-coherent, full-field optical technique used to measure the shape, displacements, and strains of mechanical structures subjected to external loads or environmental changes. Particularly valuable in experimental mechanics, 3D DIC enables precise analysis of deformation by capturing the movement of a surface pattern using two calibrated cameras from different perspectives. Through image correlation algorithms, the displacement vectors in all three directions (the in-plane: $u$, $v$; the out-of-plane: $w$) can be calculated by tracking changes in the pattern across successive images. From these displacements, full-field strain components ($\varepsilon_{xx}$, $\varepsilon_{yy}$, $\varepsilon_{xy}$) are derived, offering detailed insight into material behaviour. This stereo technique is prized for its high spatial resolution, ability to capture complex deformation fields, and suitability for real-time monitoring across a wide range of materials and loading conditions[14].

To ensure the stability and repetitiveness of the measurement, the same cameras were utilized for DIC and for shearography. The key difference was, that during the DIC measurement one arm of the interferometers was blocked to eliminate double imaging. Cameras were calibrated with Correlated Solutions 7 mm calibration target based on a set of 40 images, which resulted in a calibration error of 0.045 pixels. Recorded data was processed using VIC-3D application[15] and provided full-field displacement and strain data. To ensure consistency of the results, for all samples subset 29 and step 1 were used, meaning that the size of tracking window was 29x29 pixels and that all parameters were calculated for every pixel in the area of interest.

### 3.3 Damage area identification

To compare specimens subjected to different impact energies, a specific strategy for damage area identification is implemented. First, the image containing raw results is cropped to ensure comparability across samples and techniques. Then, to eliminate the global deformation caused by four-point bending, a compensation algorithm is applied[16,17]. This algorithm is based on a 2D polynomial fit (with the second order in the vertical direction, the first at the horizontal) which can be imagined as a shape of a parabolic cylinder. It isolates damage-related deformation by removing the global deformation inflicted by the bending effect.

Next, two mean values and their standard deviations are calculated from a healthy region of the sample. Based on these statistics, a threshold is defined as three times the mean value. Any data points exceeding this threshold are classified as part of the damaged area. This approach enables the detection of damage that would otherwise be obscured by the overall sample deformation. Finally, the area of the identified damage is calculated to provide a quantitative measure, allowing for comparison across different specimens.

## 4. RESULTS AND DISCUSSION

Below are the results for the specimen subjected to the highest impact energy of 45.89 J. The sample is tested under four-point bending, with damage monitored using both digital image correlation and shearography techniques. The first set of results presents strain maps corresponding to $\varepsilon_{xx}$, while the second set focuses on the $\frac{\partial w}{\partial x}$ maps.

It is important to note that the scales in Figure 3 and Figure 4 differ. This discrepancy arises because shearography, in the current study, provides phase data (in radians), which is not recalculated to the strain due to difficulties with tracking the zero order fringes during the increasing mechanical load. Therefore, in this study numerical values such as thresholds or specific strain magnitudes cannot be directly compared between DIC and shearography results. In future work, additional postprocessing procedures will be implemented to convert shearographic phase data into real physical units, enabling direct quantitative comparisons.

A notable difference between the two techniques is the appearance of two vertical lines in the DIC strain maps. These lines correspond to the material features associated with the fibre layup near the sample's front surface. This is not indicative of a defect but rather highlights the material's manufacturing features. Interestingly, this feature is only captured by DIC at relatively higher loads, highlighting the value of multimodal measurement approaches for comprehensive damage assessment.

Additionally, the presence of a strain gauge mounted near the left edge of the sample reduced the effective measurement area in the DIC analysis. The gauge obstructed the application of a random speckle pattern, which is essential for accurate DIC measurements, and therefore this region had to be excluded from analysis to avoid computational errors.

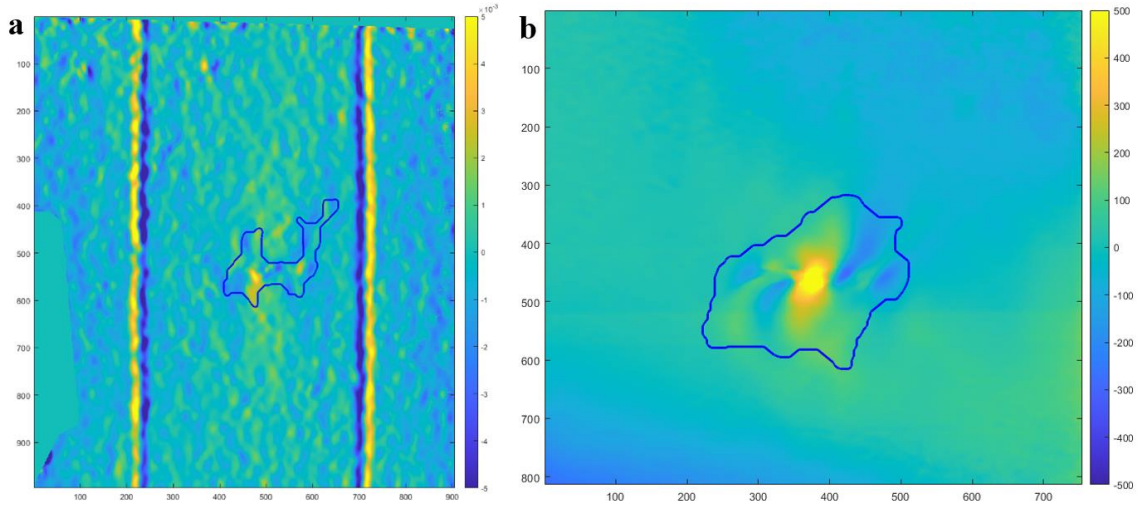


Figure 3: (a) $\varepsilon_{xx}$ strain map [-] obtained by DIC, with the damaged area outlined in blue, (b) Phase map of $\frac{\partial u_x}{\partial x}$ [rad] measured by shearography, proportional to $\varepsilon_{xx}$, with the damaged area similarly outlined in blue.

From Figure 3(a), the area of the marked damage identified by DIC is estimated to be approximately 200 mm². In contrast, the damaged region identified by shearography (Figure 3(b)) covers an area of about 540 mm². Both images were recorded under the same applied load of 2200 με in $\varepsilon_{yy}$ direction. This discrepancy can be attributed to the higher sensitivity of shearography, which is capable of detecting smaller deformation gradients. As a result, shearography highlights regions that may not yet meet the damage threshold defined by DIC but are still affected.

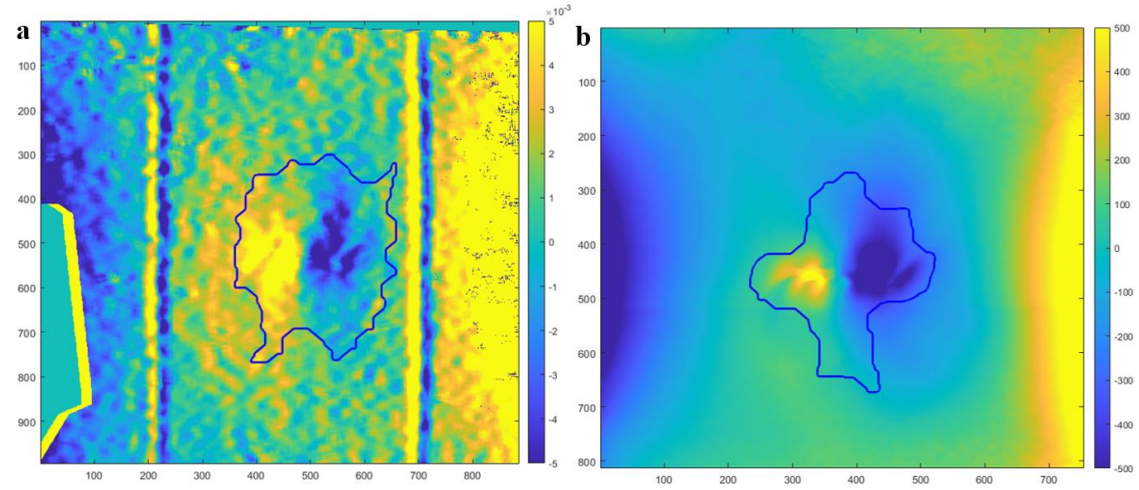


Figure 4: (a) $\frac{\partial w}{\partial x}$ map obtained by DIC, with the damaged area outlined in blue, b) Phase map of $\frac{\partial w}{\partial x}$ measured by shearography, proportional to $\frac{\partial w}{\partial x}$, with the damaged area similarly outlined in blue.

In the case of the $\frac{\partial w}{\partial x}$ map, as shown in Figure 4(a), the sensitivity of DIC to the damage increases significantly, now indicating that nearly 1000 mm² of the area is affected. In comparison, shearography detects the damaged area of approximately 570 mm², which is consistent with the area previously identified in the $\varepsilon_{xx}$ results. The load remains the same as before, approximately 2200 με in $\varepsilon_{yy}$ direction. This discrepancy suggests that the thresholding algorithm used for DIC may require further calibration, as the detected damage area differs substantially from those obtained using other methods.

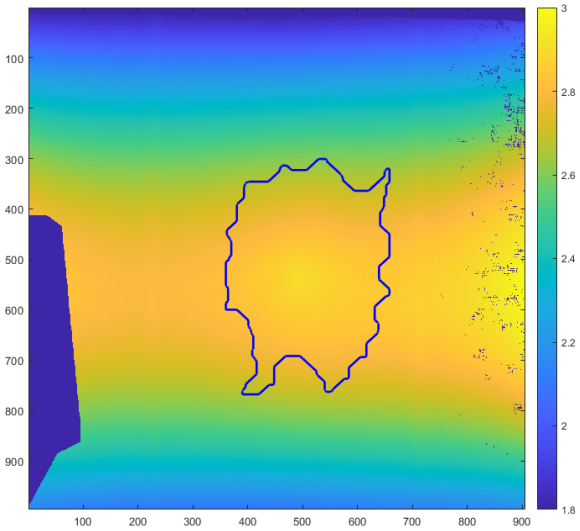


Figure 5: Out-of-plane displacement map [mm] with damage area taken from $\frac{\partial w}{\partial x}$. Presented specimen dimension is in pixels.

In Figure 5, the out-of-plane displacement map is presented, with the same damaged region indicated as previously identified in the $\frac{\partial w}{\partial x}$ map. This highlights the importance of post-processing algorithms, as such damage would not be detectable by analysing the raw W (displacement) maps alone.

## 5. CONCLUSIONS

In this study, the digital image correlation and shearography results for one of the analysed CFRP samples were presented. Both techniques provided very interesting and profound results which were aligned with the preliminary expectations: shearography technique detected smaller damage under smaller load then DIC, while DIC handled bigger changes in load then DIC. It was confirmed that four-point bending is a promising loading technique which allows to detect the impact damage in different samples. Some results and issues will need to be better studied and additional work is initiated to complement this study.

## ACKNOWLEDGEMENTS

This work was supported by the Polish National Agency for Academic Exchange (NAWA) under the PROM Programme – International scholarship exchange of PhD candidates and academic staff (Project NAWA PROM PW 2024 No. BPI/PRO/2024/1/00013/U/00001).

This study is also based upon work from COST Action HISTRATE, CA21155, supported by COST (European Cooperation in Science and Technology).

## REFERENCES


[1] Anisimov, A. G., Serikova, M. G. and Groves, R. M., "3D shape shearography technique for surface strain measurement of free-form objects," Appl. Opt., AO **58**(3), 498–508 (2019).

[2] Wang, B., Zhong, S., Lee, T.-L., Fancey, K. S. and Mi, J., "Non-destructive testing and evaluation of composite materials/structures: A state-of-the-art review," Advances in Mechanical Engineering **12**(4), 168781402091376 (2020).

[3] Malesa, M., Kowalczyk, P., Dymny, G., Skrzypczak, P., Salbut, L. and Pakula, A., "Hybrid GI-DIC measurement procedure for hierarchical assessment of strain fields," Measurement **134**, 83–88 (2019).

[4] Hampson, P. and Moatamedi, M., "A review of composite structures subjected to dynamic loading," International Journal of Crashworthiness - INT J CRASHWORTHINESS **12**, 411–428 (2007).

[5] Pascual-Francisco, J. B., Barragán-Pérez, O., Susarrey-Huerta, O., Michtchenko, A., Martínez-García, A. and Farfán-Cabrera, L. I., "The effectiveness of shearography and digital image correlation for the study of creep in elastomers," Mater. Res. Express **4**(11), 115301 (2017).

[6] Tao, N., "Shearography non-destructive testing and defect characterisation of thick composite structures" (2023).

[7] Holmes, J., Sommacal, S., Das, R., Stachurski, Z. and Compston, P., "Digital image and volume correlation for deformation and damage characterisation of fibre-reinforced composites: A review," Composite Structures **315**, 116994 (2023).

[8] Tao, N., Anisimov, A. G. and Groves, R. M., "Spatially modulated thermal excitations for shearography non-destructive inspection of thick composites," Optical Measurement Systems for Industrial Inspection XII, P. Lehmann, W. Osten, and A. Albertazzi Gonçalves, Eds., 29, SPIE, Online Only, Germany (2021).

[9] Gryzagoridis, J., Findeis, D. and Vukeya, N., "Vacuum excitation in shearographic NDT," Insight - Non-Destructive Testing and Condition Monitoring **49**, 98–101 (2007).

[10] "Characterizing the Properties of Tissue Constructs for Regenerative Engineering.", [Encyclopedia of Biomedical Engineering], Elsevier, 537–545 (2019).

[11] Hun, M., Chabot, A. and Hammoum, F., "A Four-Point Bending Test for the Bonding Evaluation of Composite Pavement," 7th RILEM International Conference on Cracking in Pavements, A. Scarpas, N. Kringos, I. Al-Qadi, and L. A., Eds., 51–60, Springer Netherlands, Dordrecht (2012).

[12] Hein, P. R. G. and Brancheriau, L., "Comparison between three-point and four-point flexural tests to determine wood strength of Eucalyptus specimens," Maderas, Cienc. tecnol.(ahead), 0–0 (2018).

[13] Anisimov, A. G. and Groves, R. M., "3D shape shearography with integrated structured light projection for strain inspection of curved objects," presented at SPIE Optical Metrology, 18 May 2015, Munich, Germany, 952517.

[14] Styk, A., Budiakivska, D., Jankowski, M., Kowaluk, T. and Kujawińska, M., "Laser tracker system supporting 3D digital image correlation with dispersed measurement fields of view," Optical Measurement Systems for Industrial Inspection XIII **12618**, 422–430, SPIE (2023).

[15] "VIC-3D.", Correlated Solutions Digital Image Correlation, <https://www.correlatedsolutions.com/vic-3d> (19 May 2025 ).

[16] Tao, N., Anisimov, A. G. and Groves, R. M., "Shearography non-destructive testing of thick GFRP laminates: Numerical and experimental study on defect detection with thermal loading," Composite Structures **282**, 115008 (2022).

[17] Tao, N., Anisimov, A. G. and Groves, R. M., "FEM-assisted shearography with spatially modulated heating for non-destructive testing of thick composites with deep defects," Composite Structures **297**, 115980 (2022).